NAVAL POSTGRADUATE SCHOOL
Monterey, California

19980417 033

DTIC QUALITY INSPECTED 4

THESIS

ANALYSIS AND DESIGN OF RETROREFLECTORS

by

Eleftherios I. Keroglou

December, 1997

Thesis Advisor: David C. Jenn

Second Reader: Phillip E. Pace

Approved for public release; distribution is unlimited.

REPORT DOCUMENTATION PAGE		*Form Approved* *OMB No. 0704-0188*

Public reporting burden for this collection of information is estimated to average 1 hour per response, including the time for reviewing instruction, searching existing data sources, gathering and maintaining the data needed, and completing and reviewing the collection of information. Send comments regarding this burden estimate or any other aspect of this collection of information, including suggestions for reducing this burden, to Washington headquarters Services, Directorate for Information Operations and Reports, 1215 Jefferson Davis Highway, Suite 1204, Arlington, VA 22202-4302, and to the Office of Management and Budget, Paperwork Reduction Project (0704-0188) Washington DC 20503.

1. AGENCY USE ONLY *(Leave blank)*	2. REPORT DATE December 1997	3. REPORT TYPE AND DATES COVERED Master's Thesis
4. TITLE AND SUBTITLE ANALYSIS AND DESIGN OF RETROREFLECTORS		**5. FUNDING NUMBERS**
6. AUTHOR(S) Keroglou, Eleftherios I.		
7. PERFORMING ORGANIZATION NAME(S) AND ADDRESS(ES) Naval Postgraduate School Monterey, CA 93943-5000		**8. PERFORMING ORGANIZATION REPORT NUMBER**
9. SPONSORING / MONITORING AGENCY NAME(S) AND ADDRESS(ES) None		**10. SPONSORING / MONITORING AGENCY REPORT NUMBER**

11. SUPPLEMENTARY NOTES

The views expressed in this thesis are those of the author and do not reflect the official policy or position of the Department of Defense or the U.S. Government.

12a. DISTRIBUTION / AVAILABILITY STATEMENT Approved for public release; distribution unlimited.	**12b. DISTRIBUTION CODE**

13. ABSTRACT *(maximum 200 words)*

The enhancement of the radar cross section (RCS) of specific bodies above their normal cross section has several military and civilian applications (e.g., sail boats and decoys). This enhancement is achieved by the use of retroreflectors. Retroreflectors are simple geometric conducting structures that concentrate the reflected wave back in the direction of incidence. They are capable of producing a high RCS over a wide range of aspect angles.

This thesis examines the RCS performance of various common retroreflector geometries. The study is performed using two computational electromagnetic simulation codes: a method of moments code and a physical optics code. The contour plots of RCS are presented for different geometries as a function of frequency. For retroreflectors composed of flat plates, the plate shape is varied to determine the affect of the plate size and profile on the RCS.

14. SUBJECT TERMS RCS, Retroreflectors			**15. NUMBER OF PAGES** 62
			16. PRICE CODE
17. SECURITY CLASSIFICATION OF REPORT Unclassified	**18. SECURITY CLASSIFICATION OF THIS PAGE** Unclassified	**19. SECURITY CLASSIFICATION OF ABSTRACT** Unclassified	**20. LIMITATION OF ABSTRACT** UL

NSN 7540-01-280-5500

Standard Form 298 (Rev. 2-89)

Prescribed by ANSI Std. 239-18

ANALYSIS AND DESIGN OF RETROREFLECTORS

Eleftherios I. Keroglou
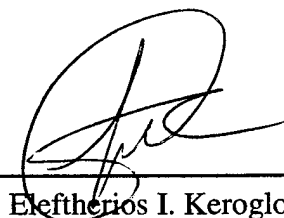Lieutenant, Hellenic Navy
Hellenic Naval Academy, 1987

Submitted in partial fulfillment of the
requirements for the degree of

MASTER OF SCIENCE IN ELECTRICAL ENGINEERING

from the
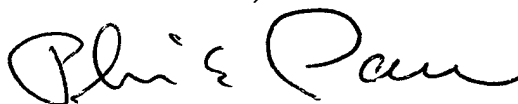
NAVAL POSTGRADUATE SCHOOL
December 1997

Author: _____
Eleftherios I. Keroglou

Approved by: _____
David C. Jenn, Thesis Advisor

_____
Phillip E. Pace, Second Reader

_____
Herschel H. Loomis, Chairman
Department of Electrical and Computer Engineering

iii

ABSTRACT

The enhancement of the radar cross section (RCS) of specific bodies above their normal cross section has several military and civilian applications (e.g., sail boats and decoys). This enhancement is achieved by the use of retroreflectors. Retroreflectors are simple geometric conducting structures that concentrate the reflected wave back in the direction of incidence. They are capable of producing a high RCS over a wide range of aspect angles.

This thesis examines the RCS performance of various common retroreflector geometries. The study is performed using two computational electromagnetic simulation codes: a method of moments code and a physical optics code. The contour plots of RCS are presented for different geometries as a function of frequency. For retroreflectors composed of flat plates, the plate shape is varied to determine the affect of the plate size and profile on the RCS.

TABLE OF CONTENTS

ACKNOWLEDGMENT

This thesis is dedicated to my wife Alkistis for her understanding and support.

I.   INTRODUCTION

The enhancement of the radar cross section (RCS) of specific bodies above their normal cross section has several military and civilian applications. There are several methods that can provide this enhancement over a specific range of aspect angles. The most common and effective is the addition of radar retroreflectors to the body. Retroreflectors are simple geometric conducting structures that concentrate the reflected wave back in the direction of incidence. They are capable of producing a high RCS over a wide range of aspect angles and frequencies.

Enhanced RCS is desired in certain commercial and military applications. The use of radar retroreflectors on small ships or sail boats can increase their RCS so that they can be easily seen and identified by other ships' radars, making navigation more safe. Another commercial application is the marking of harbor channels by mounting radar retroreflectors on buoys. This allows all ships that enter the harbor to identify and verify their course through the harbor from safe distances and depths, especially at night, thereby reducing the possibility of an accident.

In addition, radar reflectors can be used for military purposes. Perhaps the most important application in this category is the decoy. Decoys are objects that create pseudo-target information in enemy radar and thereby confuse and mislead the enemy. The payoff is that a high cost weapon will be expended against a low cost decoy. Furthermore, the real attack can approach from a different direction than that of the decoy. Retroreflectors are also used on stealth aircraft to increase their RCS in certain circumstances. They include air-to-air refueling and the masking of the true RCS when operating the aircraft in the open.

The purpose of this thesis is to examine the RCS performance of different retroreflector geometries. The RCS is computed using computational electromagnetic (CEM) codes, which are reliable, low cost and convenient computer simulation tools for scattering analysis. The RCS of commonly used retroreflector geometries is calculated at specific frequencies, using two CEM codes: (1) the method of moments code **Patch**[1] from Sandia Labs, and (2) the physical

---

[1] Computer code names will appear in boldface type.

optics code **Xpatch** from Demaco. These codes take input files
with geometry information and calculate their RCS. The
results are loaded into MATLAB for presentation and
visualization. In many cases the data are presented in two
dimensional contour plots, which clearly reveal the
retroreflector's ability to provide relatively high RCS over
a large spatial sector. The performance of different
geometries is investigated as a function of frequency. For
retroreflectors composed of flat plates, the plate shape is
varied to determine the affect of the plate size and profile
on the RCS.

Chapter II provides general information about
retroreflectors: their types and general characteristics and
common applications. Chapter III contains a description of
the codes **Patch** and **Xpatch** and information on the
electromagnetic calculations they perform. Chapter IV
provides the results, comparisons of data and comments on
these results. Finally, Chapter V summarizes this research
and presents conclusions.

II. RETROREFLECTORS

In this chapter, definitions and the fundamental characteristics of retroreflectors are introduced.

A. RADAR CROSS SECTION

1. Definition

The radar cross section σ of a target, or RCS as it is commonly referred to, is defined as the ratio of the target's effective isotropically reflected power to the incident power density. A general expression is

$$\sigma = 4\pi \frac{\text{Reflected Power / Unit Solid Angle}}{\text{Incident Power / Unit Area}}. \tag{1}$$

Mathematically RCS is defined by

$$\sigma = \lim_{R\to\infty} \left[4\pi R^2 \frac{|\vec{E}_s|^2}{|\vec{E}_i|^2} \right] \tag{2}$$

where, $\vec{E}_s$ and $\vec{E}_i$ are the scattered and incident electric field intensities respectively, and R is the distance between the radar and the target. The radar cross section has units of area but is frequently presented in decibels relative to a square meter, dBsm

$$\sigma, dBsm = 10\log_{10}(\sigma, m^2). \tag{3}$$

2. Characteristics

Radar cross section depends on several factors. They include the frequency and polarization of the incident wave and the target aspect (that is, the orientation of the target as viewed from the radar).

Although from Equation 2 it appears that RCS depends on the square of the distance R, for a radar in the far zone of the target, the scattered electric field intensity $\vec{E}_s$ varies approximately as $1/R$. Therefore, in the target far zone σ becomes range independent.

There is a high dependence of the target scattering on the incident wave frequency. In general, there are three frequency regions where the RCS of any body has distinctly different features. These are the low-frequency, resonance and high-frequency regions.

a. Low-frequency Region

In the low-frequency region the target size is small compared with the wavelength. That means if the target length is ℓ, then $k\ell \ll 1$ where k is the wave number, defined as

$$k = \frac{2\pi}{\lambda} \tag{4}$$

and λ is the wavelength. In this region RCS varies as λ^{-4} and the exact shape of the target is not important. This region is also called *Rayleigh* region. Bodies tend to scatter isotropically in this region, although at quite a low level.

b.   Resonance Region

In the resonance region $k\ell \approx 1$. For these frequencies the induced current varies in phase across the body and the RCS is oscillatory with frequency. This region is also called *Mie* region, named after the researcher who originally solved the sphere scattering problem.

c.   High-frequency Region

In the high-frequency region the target size is large compared with the wavelength, that is, $k\ell \gg 1$. Within this region, which is also called the *optical* region, the scattered field is strongly dependent on the angle. Figure 1 shows these three regions for the case of the target being a sphere. The RCS has been computed using the Mie series [Ref. 1].
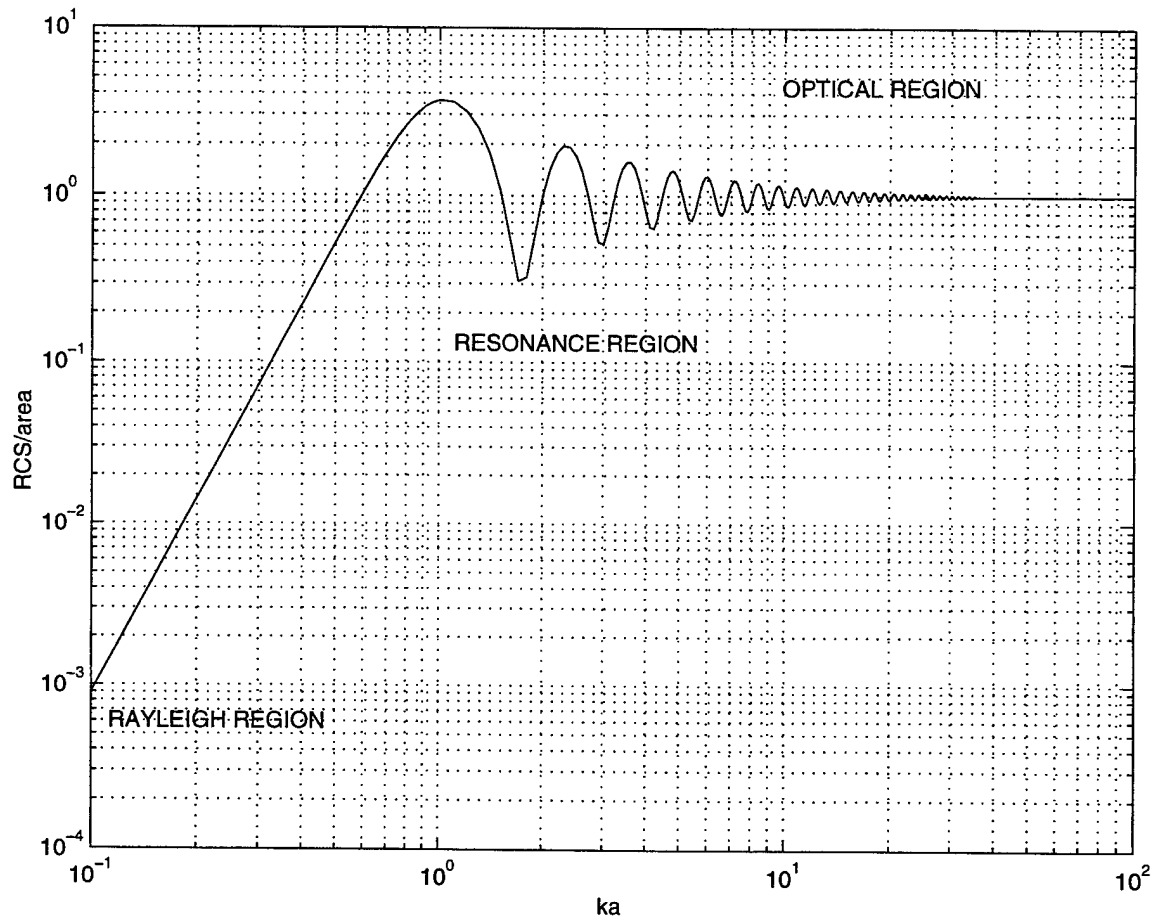
Figure 1. RCS and frequency regions of a sphere (After Ref.[1]).

B.   REFLECTORS

Retroreflectors (or retrodirective reflectors) have been designed to reflect a signal towards the source.over a wide range of incident wave angles. They are used in order to enhance the RCS of specific targets such as navigation buoys, sail boats, small drones and weather balloons. The important property is that they reflect the incident signal back in the same direction, thus providing a much larger signal than if the incident wave were specularly reflected. An example is shown in Figure 2. The monostatic return from a tilted flat plate is small, but if a second plate is added, the structure becomes a retroreflector and the monostatic RCS is enhanced as illustrated. This is an example of one of the most common types of retroreflectors: the corner reflector.

Since the retroreflector reflects the incident rays back in the same direction, they are effective only for monostatic radar cases and for special bistatic radar cases where the transmitting and receiving antennas are very close. In general, the monostatic RCS of a large flat

structure based on the physical optics approximation [Ref. 1] is given by

Low
Scatter

High
Scatter
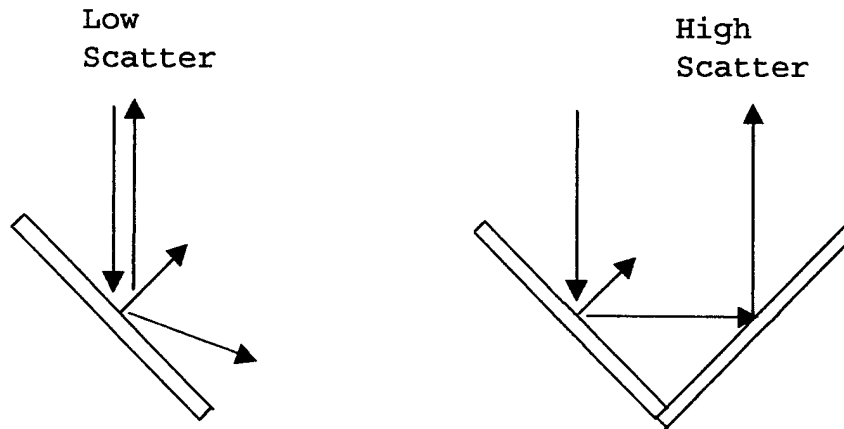
Figure 2. The monostatic RCS is enhanced with the addition of a second plate.

$$\sigma(\phi,\theta) \approx 4\pi \left(\frac{A_e(\phi,\theta)}{\lambda} \right)^2 \qquad \text{(5)}$$

where A_e is the effective area of the reflector presented to the source. The angle θ is measured from the normal to the surface. In many cases this formula is an acceptable approximation for the RCS of structures that are not flat.

There are several types of corner reflectors, but the most common are the dihedral and the trihedral corner reflectors which are discussed in the following subsections.

10

1.   Dihedral Corner Reflectors

A dihedral corner reflector can be built by joining two reflecting surfaces (such as rectangular or triangular plates) at right angles. An example of a dihedral consisting of two rectangular plates is shown in Figure 3.
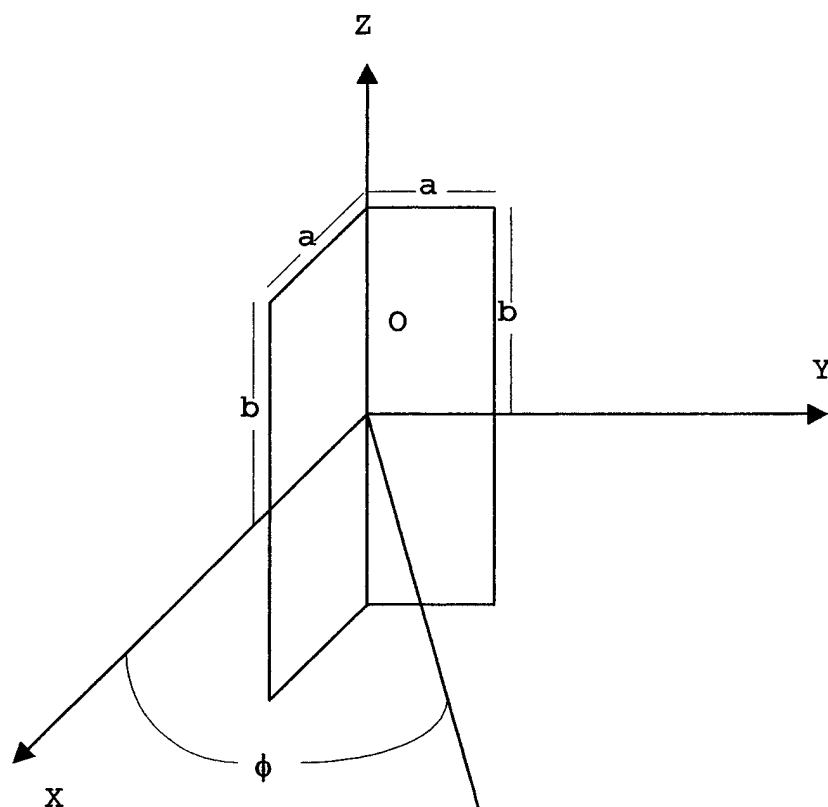
Figure 3. A dihedral corner retroreflector consisting of two rectangular plates (After Ref. [2]).

An incident wave approaching in a plane perpendicular to the intersection line (i.e., $x-y$ plane) will be

11

specularly reflected twice thus giving a high reflected wave. The basic limitation of a dihedral in performing as an efficient retroreflector is that the incident wave must be restricted near to the plane transverse to the intersection of the plates and the bisector of the corner angle. That is, within a few degrees of the $x-y$ plane and $\phi = 45°$ in Figure 3.

The RCS of the rectangular dihedral is approximately given by Equation 1 where the effective area in the vicinity of $\theta = 90°$ is

$$A_e = 2ab\sin(\pi/4 + \phi).$$
(6)

Thus, an estimate of the RCS of this corner reflector is approximately

$$\sigma \approx \frac{16\pi a^2 b^2 \sin^2(\pi/4 + \phi)}{\lambda^2}.$$
(7)

The horizontal coverage (range of ϕ in a plane transverse to the common edge) of this type of reflector is about 90 degrees centered in the bisecting plane. The limitation of the dihedral corner reflectors can be overcome by incorporating a third plate at right angles to the first two, i.e., the trihedral corner reflector.
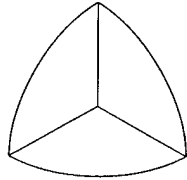
2. Trihedral Corner Reflectors

A trihedral corner reflector can be formed by adding a third reflecting surface perpendicular to the first two. The spatial sector of high RCS increases to a solid angle of about $(\pi/2)^2$ steradians ($\pi/2$ radians in each of the two principal planes). Figure 4 illustrates three different types of trihedral corner reflectors: triangular, circular and rectangular, along with approximate formulas to calculate their RCS. From these formulas it is easily seen that a rectangular plate provides a factor of nine times larger RCS than that of a triangular plate.

In order for a reflector of this category to work as a retroreflector, incident rays must be reflected back from all three surfaces. To obtain a larger RCS, the effective area A_e of the collection of plates must be increased. The maximum occurs when the incident wave is parallel to the axis of symmetry of the reflector. In a ground based application that means if the incident wave is expected along the horizon (slightly above the horizontal), then the trihedral must not be mounted with any of the three surfaces in the horizontal plane.
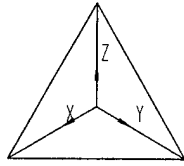
$$\sigma = \frac{1}{3}\frac{4\pi\ell^4}{\lambda^2}$$

$$\sigma = 15.6\frac{\ell^4}{\lambda^2}$$
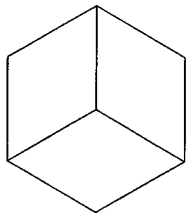
$$\sigma = 3\frac{4\pi\ell^4}{\lambda^2}$$

Figure 4. Triangular, circular and rectangular corner retroreflectors along with their formulas. The quantity ℓ is the common edge length (After Ref.[3]).

14

The approximate effective area of a trihedral can be determined by projecting the surfaces onto a plane perpendicular to the viewing direction. For the case of a triangular plate trihedral, Figure 5 shows how the effective area can be determined. This area is represented by the shaded part. After A_e is determined, the RCS can be estimated using Equation 1.
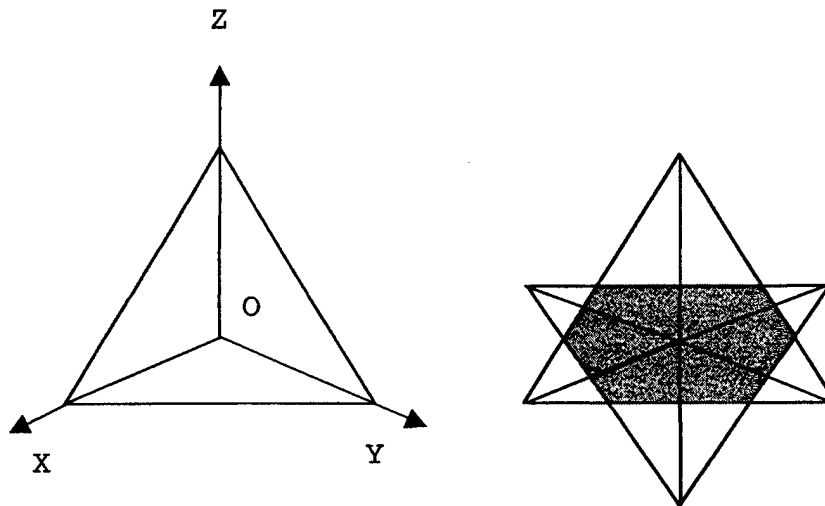
Figure 5. Determination of the effective area of a triangular plate trihedral (After Ref. [3]).

For a square plate trihedral, the RCS can be calculated as a function of the spherical angles θ and ϕ. For values of θ and ϕ near the symmetry axis the result is

$$\sigma(\theta,\phi) \approx \frac{4\pi}{\lambda^2} \cos^2\theta \, (4-\cot\phi)^2 \ell^4 \qquad (8)$$

where ℓ is the side length. In a similar manner, for a triangular corner reflector, the RCS can be calculated by

$$\sigma(\theta,\phi) \approx \frac{4\pi}{\lambda^2} \ell^4 \Big[\cos\theta + \sin\theta\,(\sin\phi + \cos\phi) - 2\big[\cos\theta + \sin\theta\,(\sin\phi + \cos\phi)\big]^{-1} \Big]^2 .$$

$$(9)$$

The above formulas are limited in application and even then do not provide accurate results in all cases. For more accurate RCS prediction computer codes must be used. Several codes that can be used to solve this type of problem are discussed in the next chapter.

III. COMPUTER CODES

A.   Patch

Patch is a method of moments triangular subdomain code that was developed by Sandia Labs. It is a Fortran computer code that is based on the solution of the electric field integral equation (EFIE). It is applicable to both electromagnetic radiation and scattering problems. It models a continuous surface by discrete triangular patches in order to handle arbitrary body shapes easily and accurately.

1.   Method of Moments (MM)

The MM is a numerical technique that is used to reduce the EFIE to a set of linear equations, and thus converts the integral equation to a matrix problem. The size of the matrix, that is, the number of the unknowns, depends on the number of the triangular patches used to represent the body.

The unknown quanity in the EFIE is the surface current distribution $\vec{J}_s$. To apply the MM, $\vec{J}_s$ is represented by a series with unknown coefficients

$$\vec{J}_s = \sum_{n=1}^{N} I_n \vec{J}_n \qquad (10)$$

17

where $\{\vec{J}_n\}$ are the basis functions. The selection of the basis functions is important. Pulses, δ functions, triangles and sinusoidals are frequently used as basis functions. In order to determine the unknown coefficients I_n, a matrix of N linear equations is formed. By exploiting the properties of the basis functions, the $\{I_n\}$ are determined and thus $\vec{J}_s$ is also determined.

After the current coefficients have been determined, the radiation patterns and the scattered fields can be computed. If the MM is properly applied, the actual current series representation will converge to the true current as the number of the basis functions is increased. A useful rule of thumb is that the edge length should not exceed 0.1λ. In general, the number of edges and unknowns is almost the same. Small differences occur due to the fact that there are more than two current coefficients associated with some edges. On the other hand, if the edge of a triangle is also the edge of the body, then there is no current flowing across it and therefore no expansion coefficient is required. **Patch** uses overlapping rooftop functions as

expansion functions $\vec{J}_n$. The current at a point on a surface triangle is the vector sum of the currents crossing the three edges weighted by their distances from the edge.
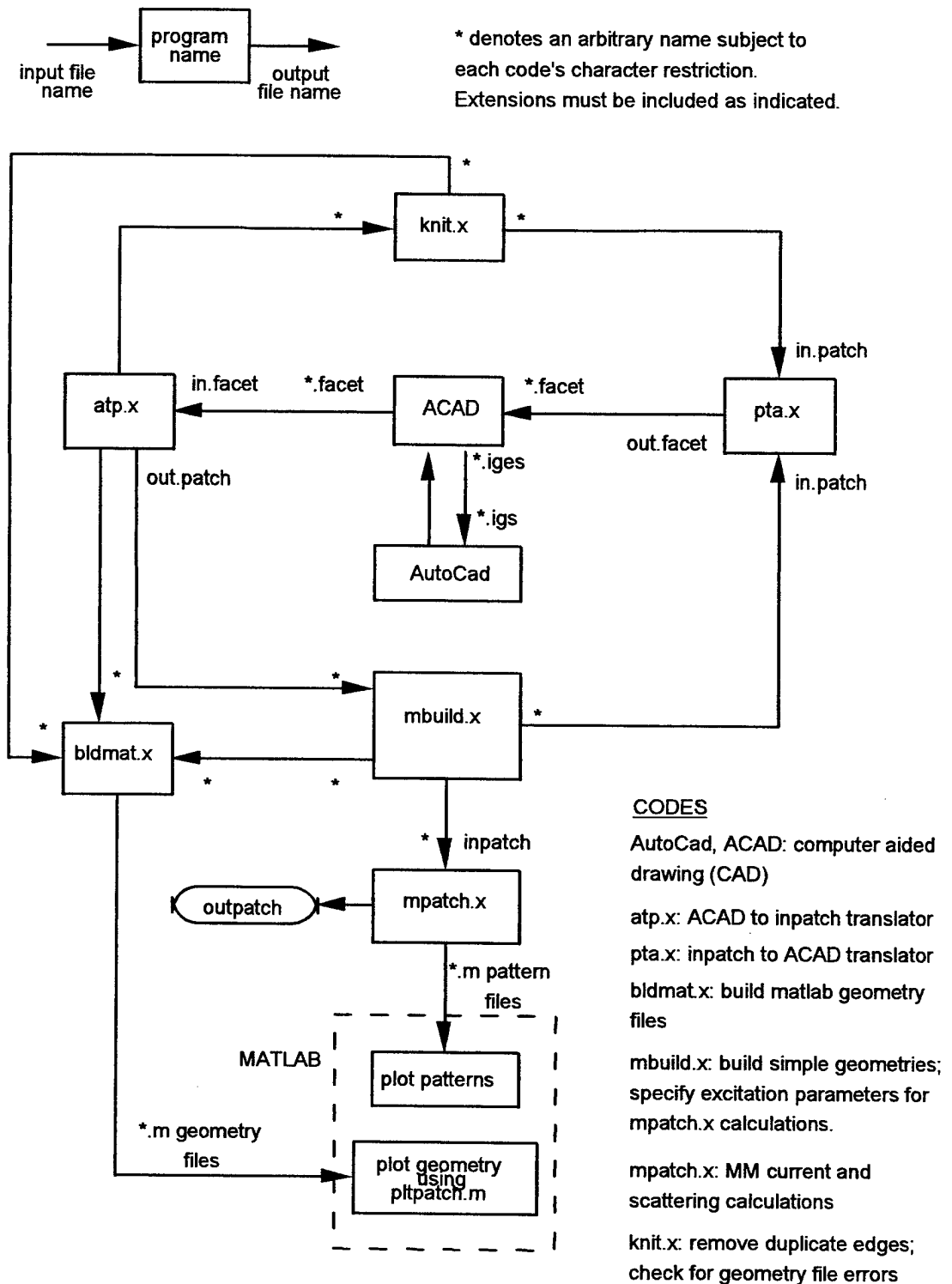
Several computer codes are used to generate facet models, perform the computational electromagnetics, and present the output data. The code relationships are summarized in Figure 6. Several output files are generated by **Patch.** They include the RCS as a function of θ and φ which can be plotted in MATLAB.

2. Program Build

Build is a program that generates faceted target bodies by joining a set of simple three-dimensional shapes. The data is written in a format that is recognized by **Patch.** **Build** is capable of generating five basic geometries: quadrilateral, cylinder, cone, disk and sphere:

(1) Quadrilateral: This is formed by specifying the coordinates of the four corners and the number of edges along two adjacent sides.

(2) Cylinder: A cylinder is formed by specifying four points. The first two points, a center point and a point on the circumference define the top face and similarly two

Figure 6. Relationships between computer codes.

CODES

AutoCad, ACAD: computer aided drawing (CAD)

atp.x: ACAD to inpatch translator

pta.x: inpatch to ACAD translator

bldmat.x: build matlab geometry files

mbuild.x: build simple geometries; specify excitation parameters for mpatch.x calculations.

mpatch.x: MM current and scattering calculations

knit.x: remove duplicate edges; check for geometry file errors

20

other points define the bottom face. The cylinder axis is defined by the two center points.

(3) Cone: A cone with finite length and open end is formed by specifying three points. These are the top, the center point of the base and a point on the circumference. The number of edges from the apex to the base and around the circumference are also specified.

(4) Disk: A disk is formed by specifying a center, a circumference and an axis point. The number of circumferential and radial edges are also required in order for the triangulation to be specified. Nonuniform segment lengths along the radial dimension can be specified.

(5) Sphere: A sphere is specified by a center point, a point on the equator of zero degrees longitude and a point at the north pole. A portion of a sphere can be specified by providing the beginning and ending angles at specific longitudes and latitudes.

3. Code Capabilities

Apart from building the shape, **Patch** provides some options to the user. Among them is the symmetry option. This option enables the user to reduce the number of computations

and thus the time required by using image planes placed on the $x=0$, $y=0$ or $z=0$ planes. These image planes can be either perfect electric conductors (PEC) or perfect magnetic conductors (PMC). By inserting a symmetry plane, for each triangular patch an image one is created. Other quanities such as voltage sources or distributed impedances follow the image properties and are taken into account automatically. Capabilities are summarized in Table 1.

Table 1. Summary of Patch Capabilities

Arbitrary Shape
 Open/Closed objects
 Modelled by triangular " patches"
   Variable patch density
   Front end for graphical composition
 Arbitrary edge multiplicity
 Non-orientable surfaces
 Symmetry planes may be included
 Multiple bodies

Surface
Basis functions yield surface currents
   Type: Wilton Rao
   Free of line and point charges
 Equivalent Thevenin circuits
 Lumped and surface impedance loading

Excitation
   Voltage sorces
   Plane waves
   Both

Calculated Quanities
 Surface currents
 Far field patterns
 Radar cross section
 Field calculations at
 general observation
 points

Frequency Domain
 Pattern loops
 Frequency loops

Apart from the above options, **Patch** has the options of entering the number of impedance loads and faces with

surface impedance loads, printing the currents and computing the field at an observation point or points. All of these options make **Patch** code a powerful and useful tool in the RCS calculation of a variety of structures.

B.   Xpatch

Xpatch[2] is a computational electromagnetics code from Demaco. It consists of high-frequency radar signature prediction codes based on the shooting and bouncing ray (SBR) technique [Ref. 4]. In this technique, a number of rays are transmitted towards a target and then traced according to geometrical optics (GO) as they bounce around within the target. When exiting the target, the scattered far field is calculated using a physical optics (PO) integration. Therefore, using the SBR technique, all bounce contributions are accounted for in the PO current calculation. Several factors such as the ray divergence and polarization are included in the tracing. There is also an option to include the first-order edge diffraction which is calculated by the physical theory of diffraction (PTD).

---

[2] All computed data and information relating to **Xpatch** was provided by Professor David C. Jenn

The code is composed of three parts: (1) the electromagnetic part which has four individual codes (**xpatch1**, **xpatch2**, **xpatch3** and **xpatch4**), (2) the CAD and visualization part, and (3) the graphical user interface (GUI). Any subcode can be used individually or as a component in the GUI. For example, in **xpatch1** the total scattered field is the coherent sum of the fields from the first and higher bounce contributions and the edge diffraction. The calculation of the total field can be done using either a PO integration or a z-buffer technique. The best choice of the method depends on the target shape. That is, if the target has a simple geometry (plate, cube, sphere, etc.) the first method is the best choice. For more complex targets (plane, missile) the z-buffer is faster. All three methods give nearly the same results for complex targets.

The codes discussed in this chapter were used to analyze the RCS of the different retroreflectors and the results are presented in the next chapter.

IV. RESULTS AND DATA ANALYSIS

In this chapter the RCS of retroreflectors comprised of three different plate shapes is computed and the results are discussed. The computation is based on both the **Patch** and **Xpatch** codes and a comparison of these two codes is given. Furthermore, the code convergence versus the number of segments is checked and, finally, a comparison is made of the RCS values from the codes and formulas given in Figure 4.

A. PLATE SHAPES

The basic retroreflector shapes that are considered in this thesis are:(1) three rectangular plates, (2) three triangular plates and (3) three circular wedge shaped plates. The plates are located in the $x-y$, $x-z$ and $y-z$ planes as shown in Figures 7, 8, and 9. All of the principal edge lengths are arbitrarily set at 10m. All data is normalized by λ^2. Thus, the RCS is given by σ/λ^2 in dB. The incident wave polarization is $\hat{\theta}$ and both the $\hat{\theta}$ and $\hat{\phi}$ receiver polarizations were computed. The shapes were tested

25
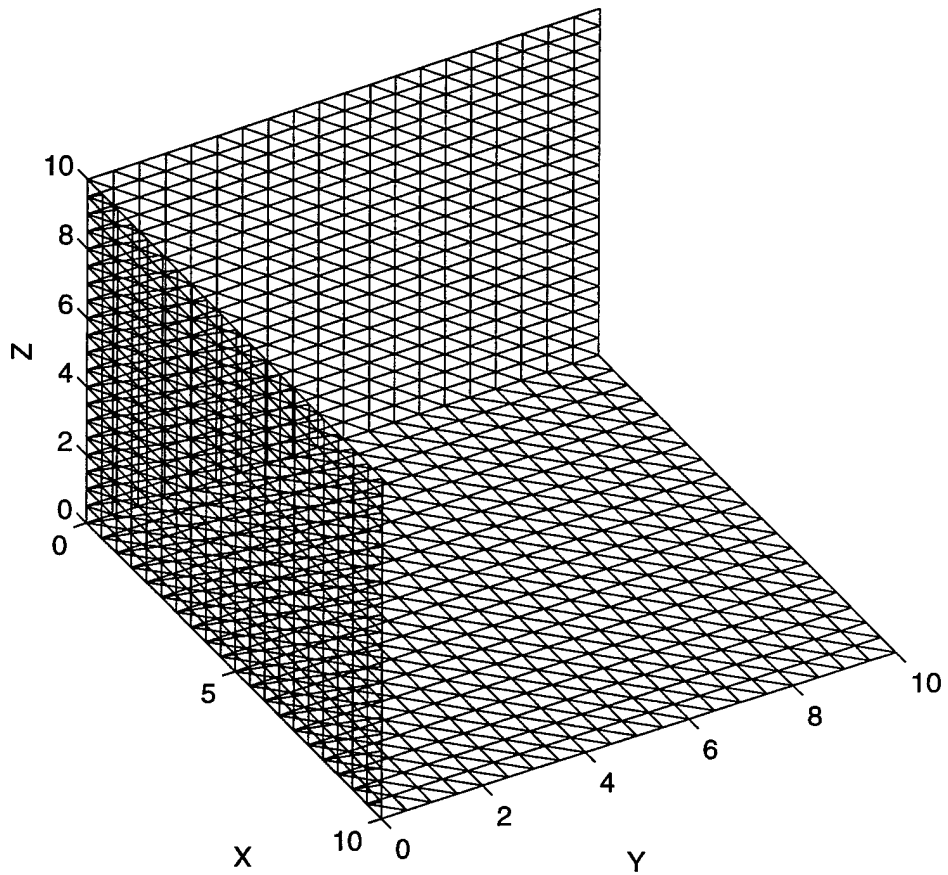
Figure 7. Three square plate geometry with 10m side length and 20 edges/side.
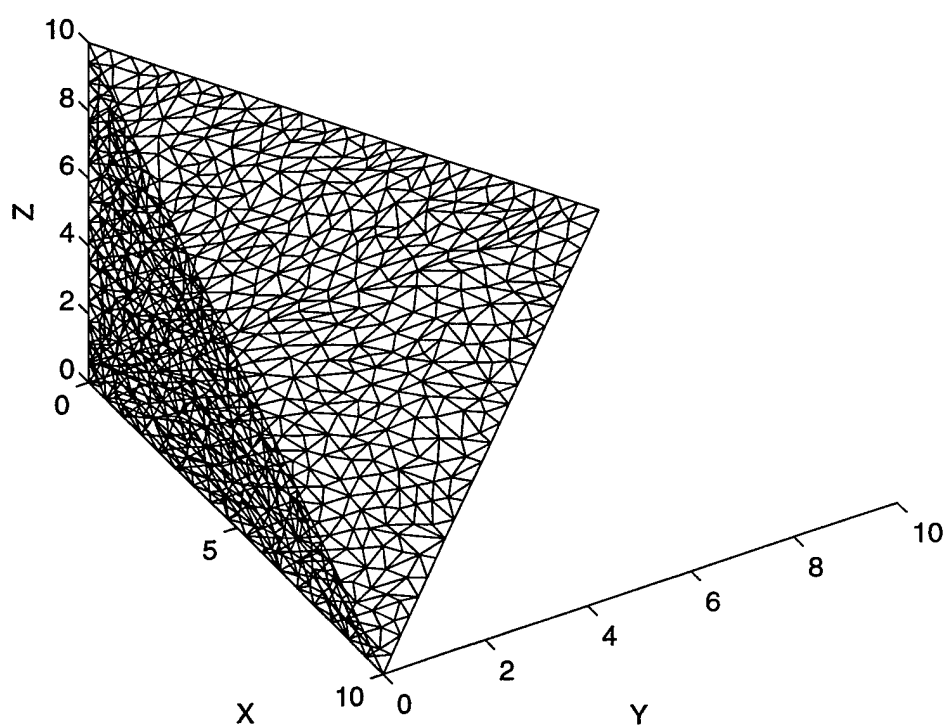
Figure 8. Three triangular plate geometry with 10m side length and 20 edges/side.
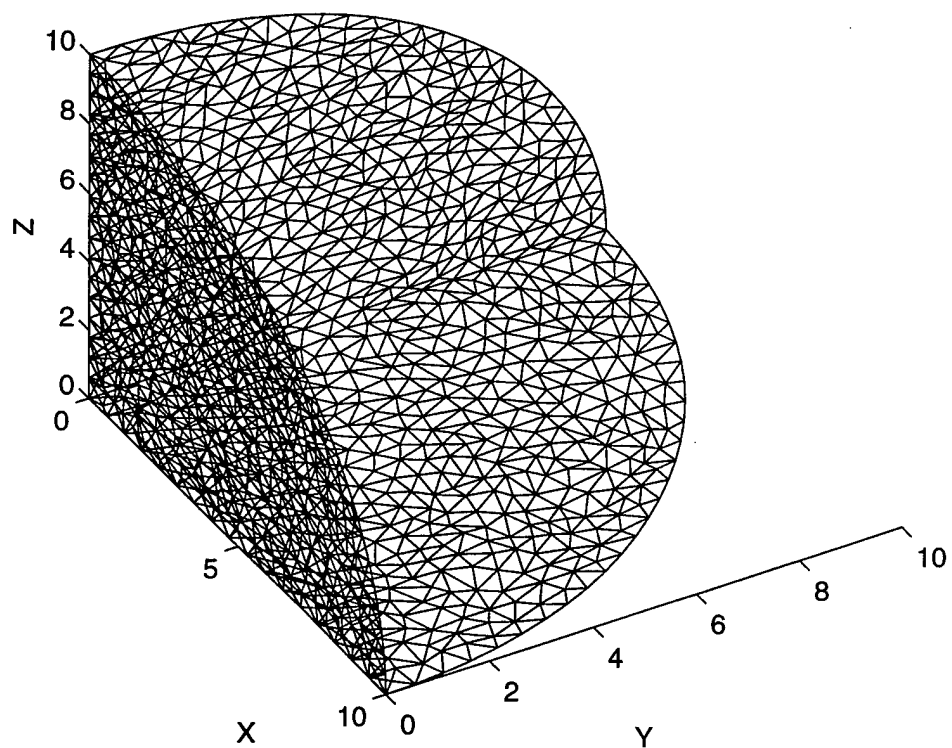
Figure 9. Three circular wedge shaped plate geometry with 10m side length and 17 edges/side.

at frequencies of 30, 60 and 120 MHz. The computational

models, that is, the number of edges per side were generated

using the CAD program ACAD. The RCS is computed over the

hemisphere where $z > 0$. This corresponds to spherical angles

$0 \leq \theta \leq 90°$ and $0 \leq \phi \leq 360°$ and direction cosines $-1 \leq u, v \leq 1$ where

$$u = \sin\theta \cos\phi ,\qquad (11)$$

$$v = \sin\theta \sin\phi .\qquad (12)$$

Contour plots were generated in direction cosine space. The

contours enclose regions where the RCS is greater than the

specified value.

At a frequency of 60 MHz, the RCS is higher in the case

of the rectangular and curved plate structures (+20 dB)

relative to the case of the triangles (+10 dB). This was

expected since the effective area of the rectangular plates

is larger than that of the triangular plates. The highest

RCS value in all three cases occurs in the first quadrant of

the $u - v$ plane $(0 \leq u, v \leq 1)$. The contour plots for these three

cases are shown in Figures 10, 11, and 12. By doubling the

frequency to 120 MHz, the RCS is also increased for all

three cases and the highest values become +30 and +20 dB

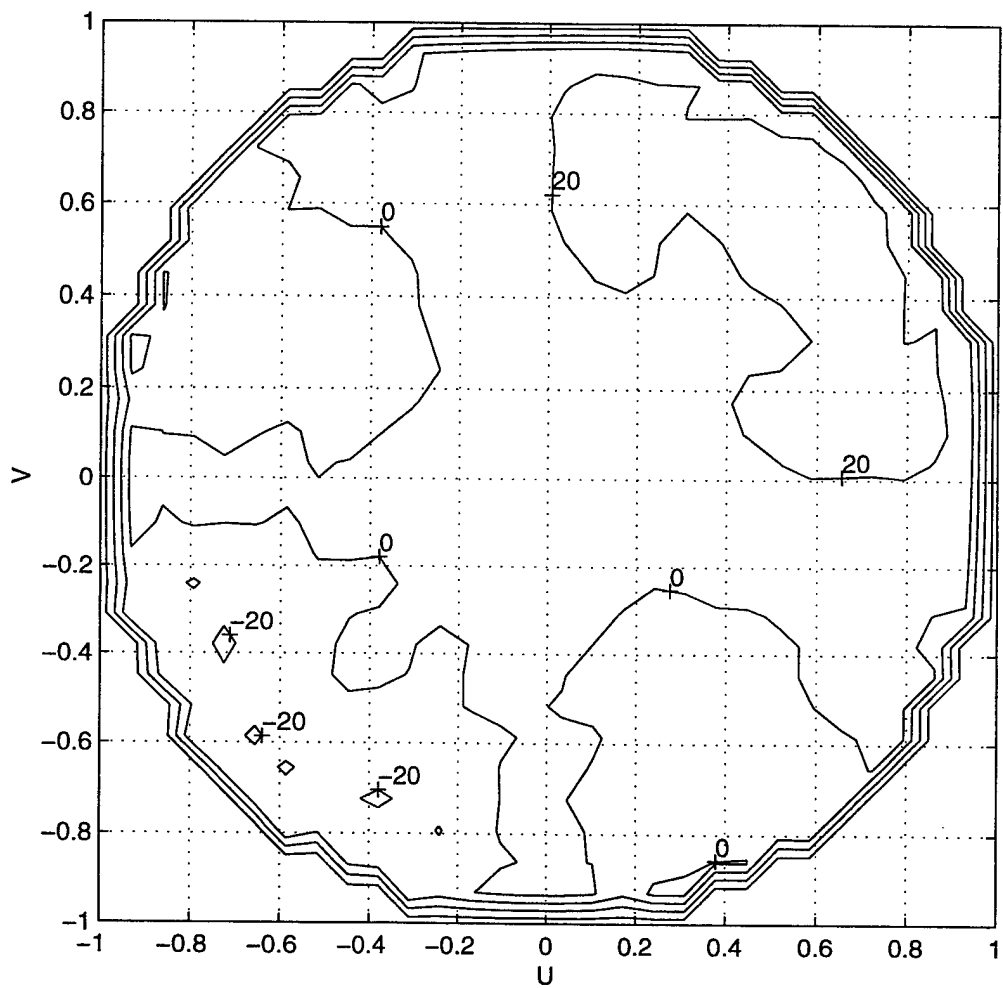respectively. The area where the highest RCS occurs remains
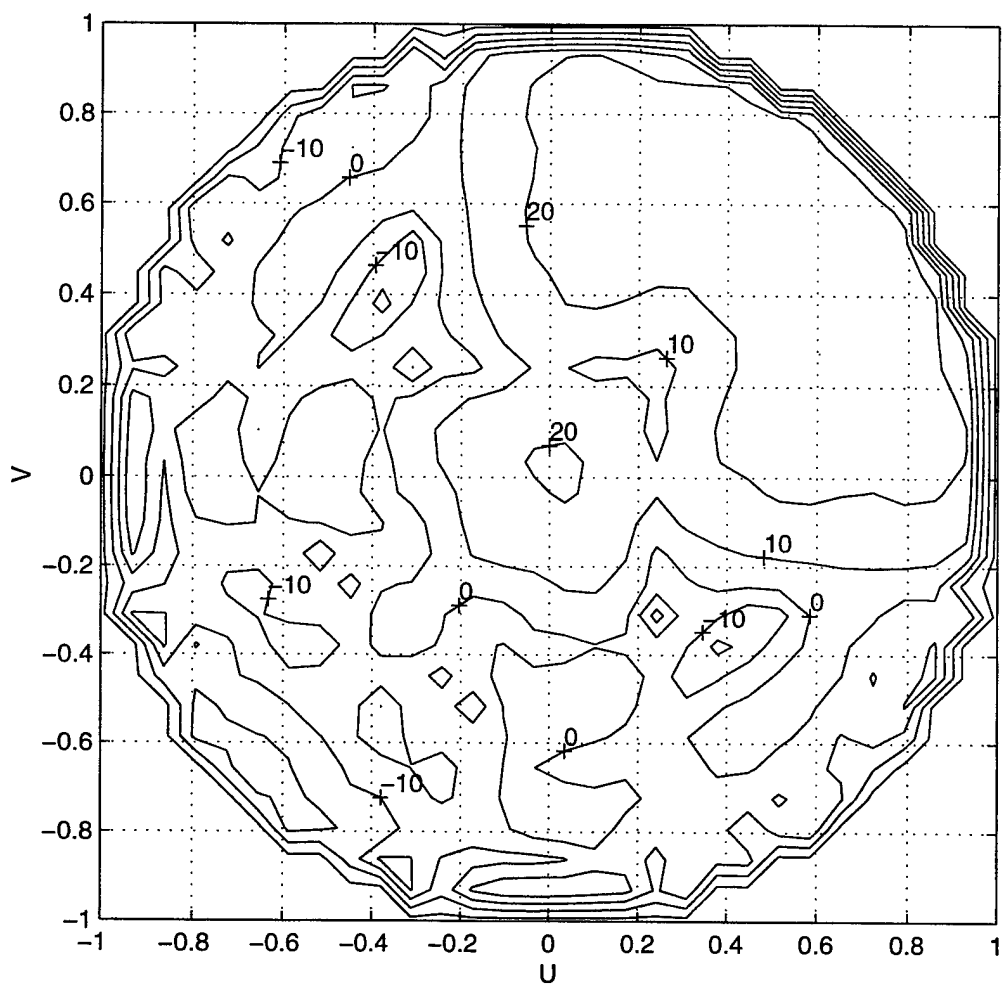
Figure 10. RCS of three rectangular plate geometry at frequency of 60 MHz and 20 edges/side using **Patch**.
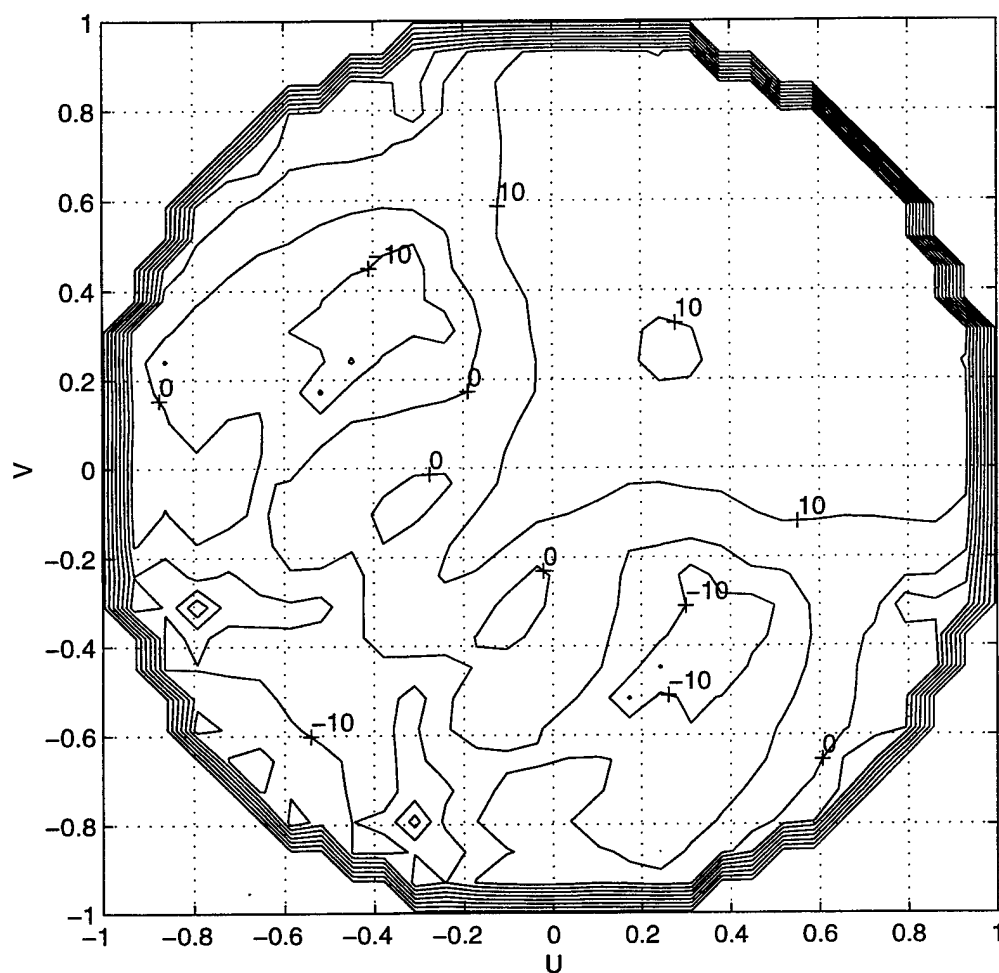
Figure 11. RCS of three triangular plate geometry at frequency of 60 MHz and 20 edges/side using **Patch**.

Figure 12. RCS of three circular wedge shaped plate geometry at frequency of 60 MHz and 17 edges/side using **Patch**.

the same as that at the frequency of 60 MHz. This was also expected since, from Equation 3, the RCS is inversely proportional to the square of the wavelength.

In addition to the three above shapes, a fourth one was also investigated. This was the octahedral shown in Figure 13 whose RCS was calculated at the frequency of 30 and 60 MHz. The octahedral can be considered as eight trihedrals with a common vertex. At the frequency of 60 MHz the highest RCS value was +20 dB and this occured in the directions shown in Figure 14.

## B.   COMPARISON OF RESULTS

RCS data were generated using both **Patch** and **Xpatch**. This was done for verification and comparison of the computational approaches. Looking at the contour plots from both codes, it is seen that they generally agree at high frequencies. The results for the case of the triangular plates at the frequency of 120 MHz are shown in Figures 15 and 16. At lower frequencies the low level contours are different although the highest RCS values remain the same. For a detailed look, several cuts were taken at angles of
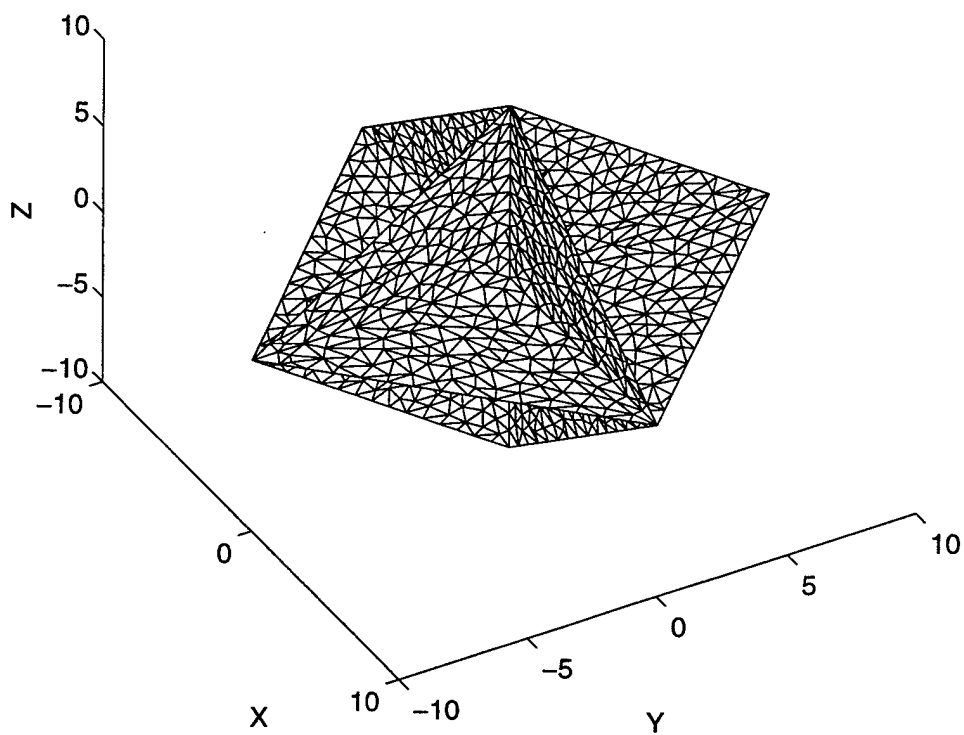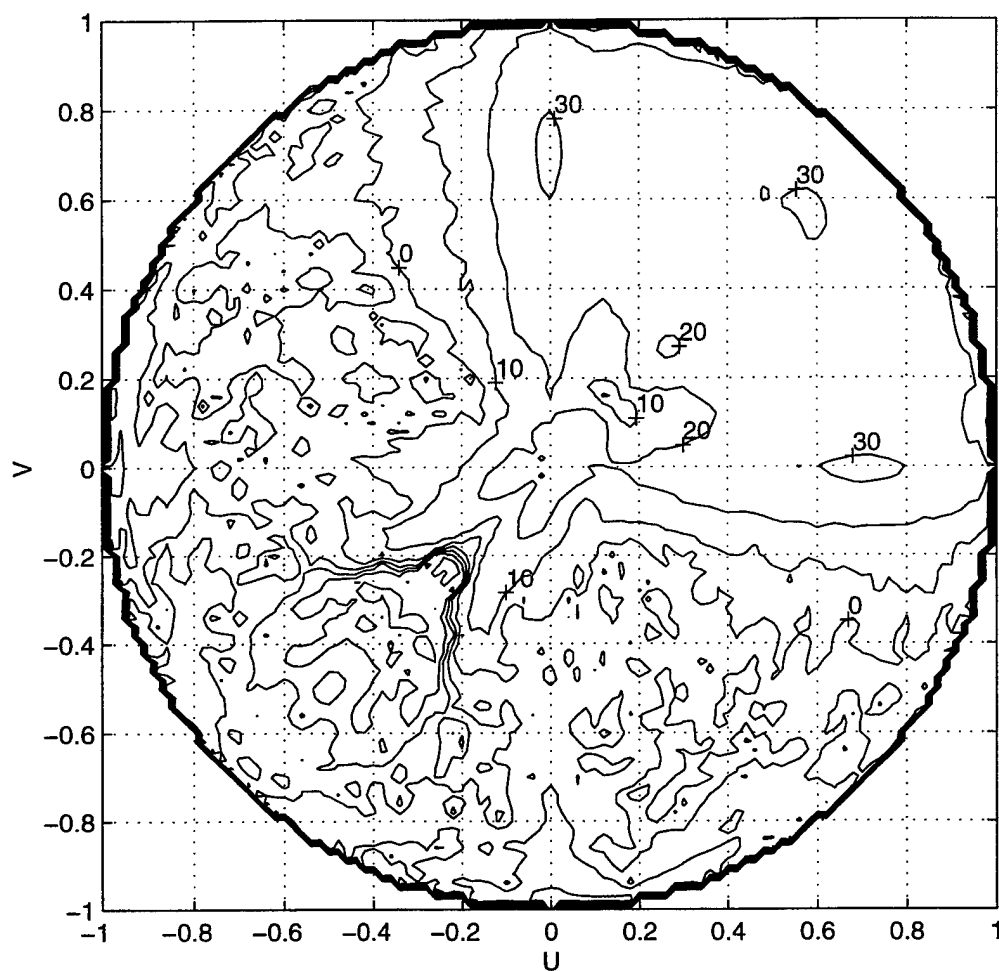
Figure 13. Octahedral geometry with 10m side length and 15 edges/side.
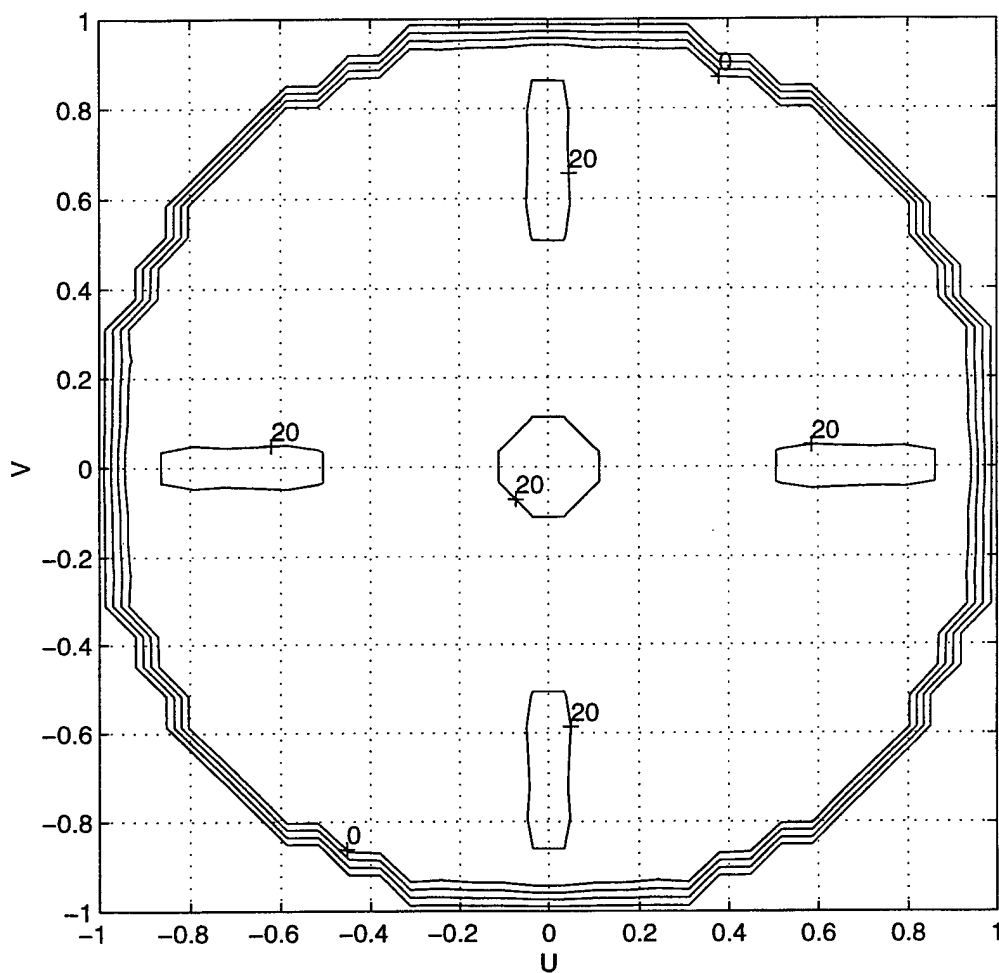
Figure 14. RCS of octahedral at frequency of 60 MHz and 15 edges/side using **Patch**.
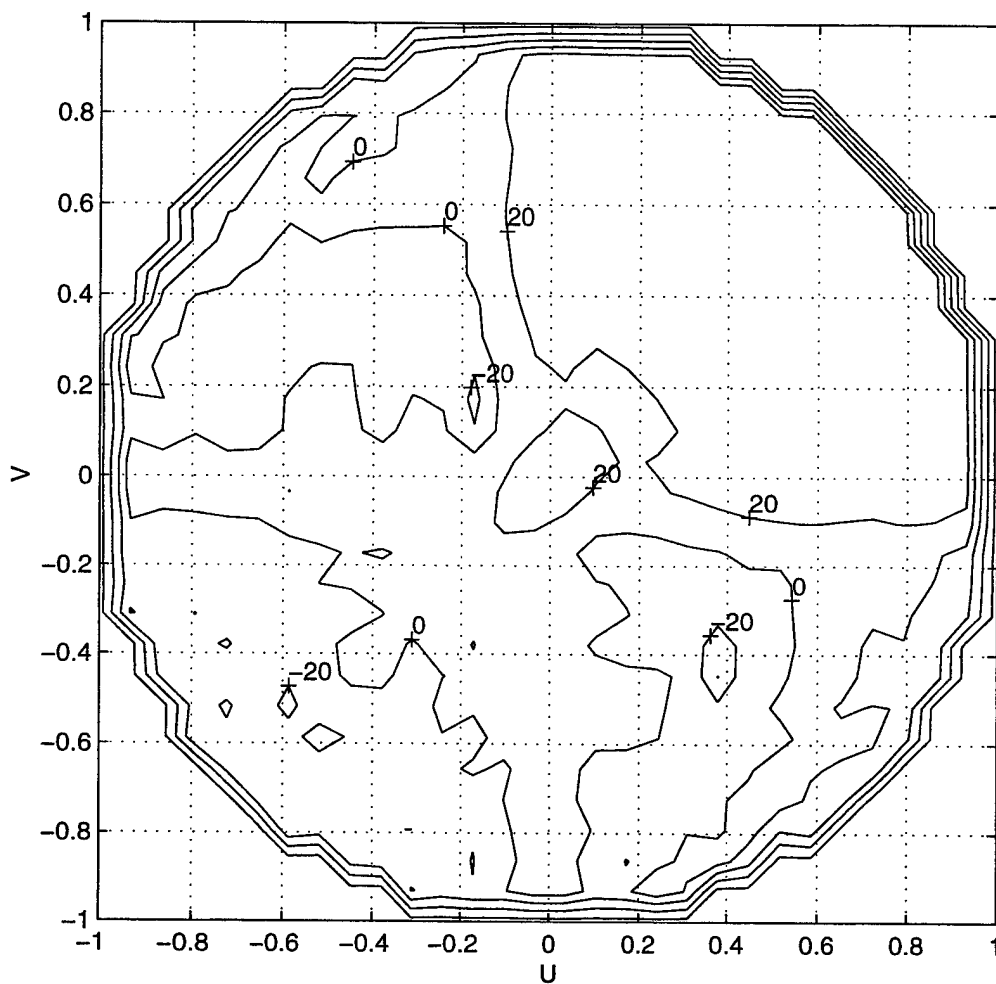
Figure 15. RCS of three triangular plate geometry at frequency of 120 MHz and 20 edges/side using **Patch**.
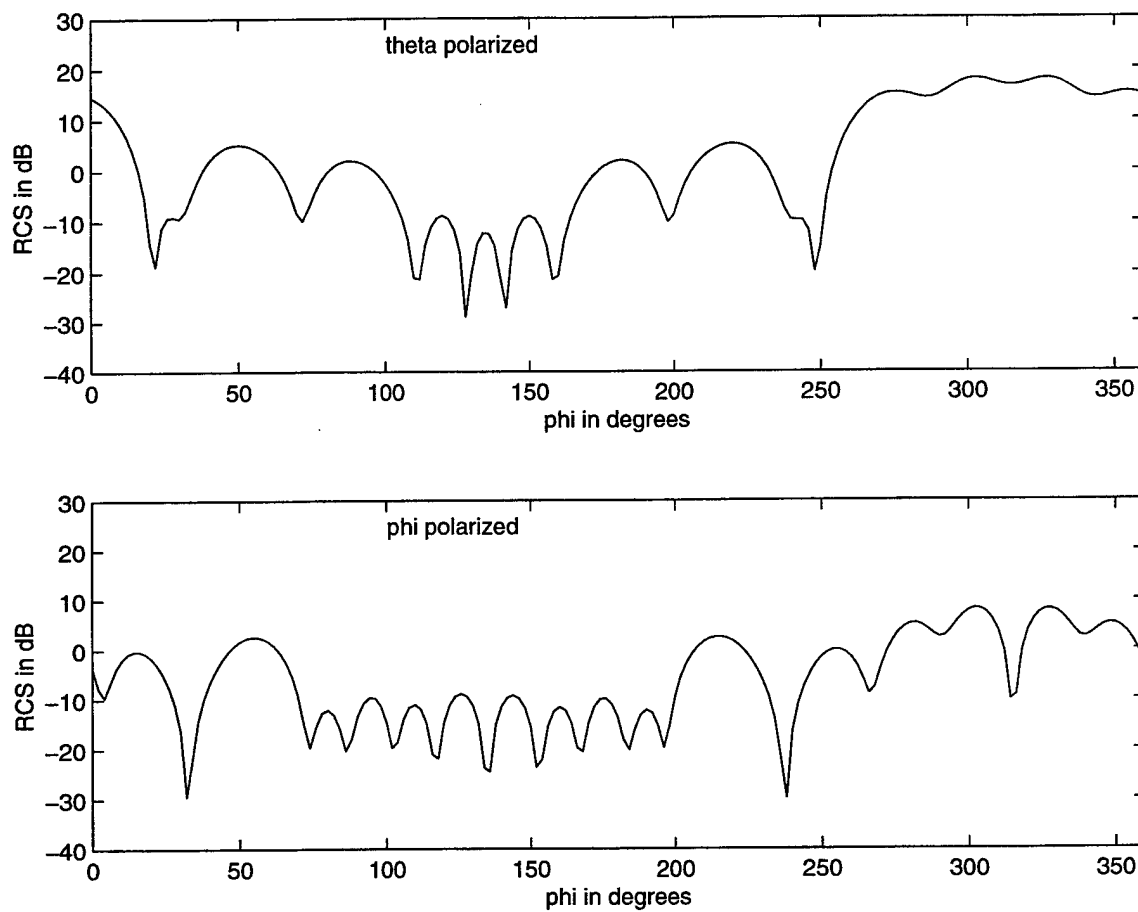
Figure 16. RCS of three triangular plate geometry at frequency of 120 MHz and 20 edges/side using **Xpatch**.

θ =30, 60 and 90 degrees. A comparison between the two codes for the triangular plate case at the frequency of 60 MHz and for $\theta = 60°$ is shown in Figures 17 and 18. The results are in agreement given that the two codes are based on different calculation methods (MM and PO). Both the θ and ϕ polarizations from **Xpatch** are very close while the ϕ polarization plot from **Patch** is much different than that of θ polarization. This is due to the fact that the **Xpatch** calculation did not include edge diffraction. As the frequency decreases, the maximum values of σ are close, but the shapes of the curves change dramatically. This is expected at low frequencies because PO and SBR are high-frequency techniques.

C.   CODE CONVERGENCE

The effect of the number of facets in the **Xpatch** model was checked. Three separate cases of plate segmentation were examined for frequencies of 30, 60 and 120 MHz: (1) for 25 edges/side, (2) for 20 edges/side and (3) for one edge/side (that is, three triangles without segmentation). The results for (1) and (3) are shown in Figures 19 and 20. From the
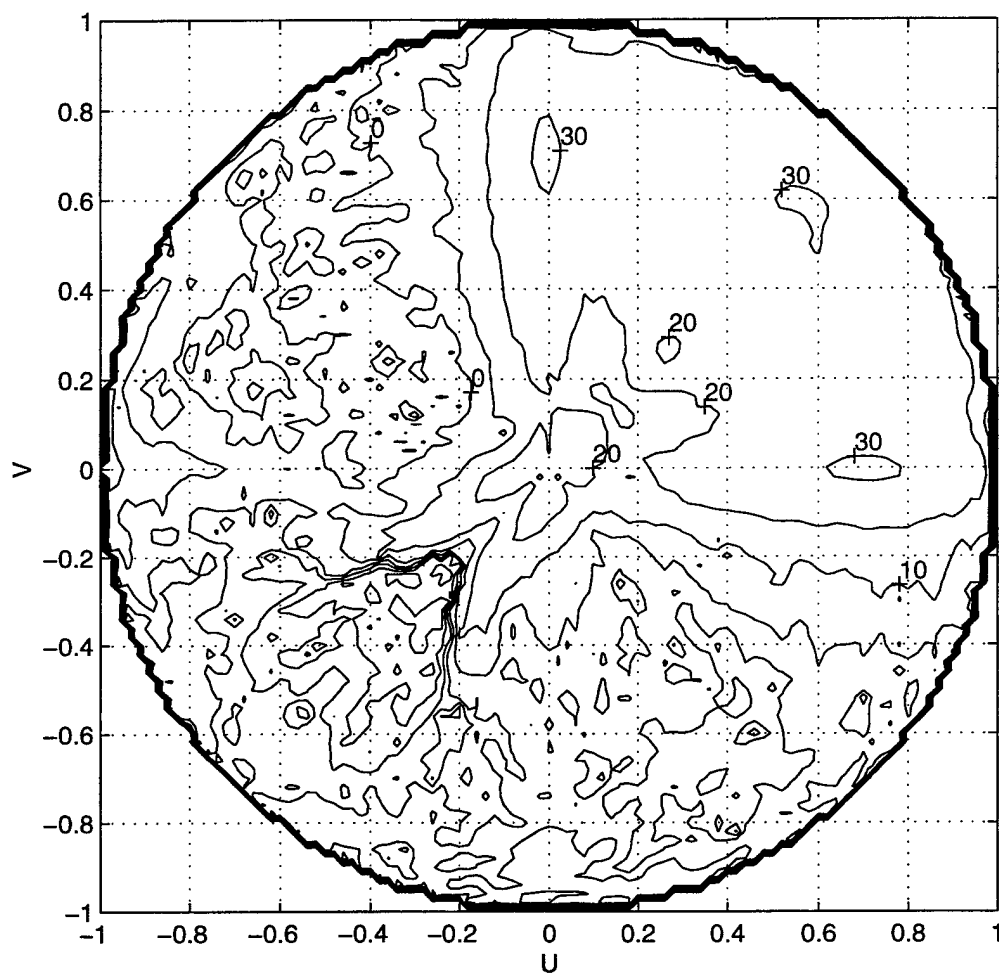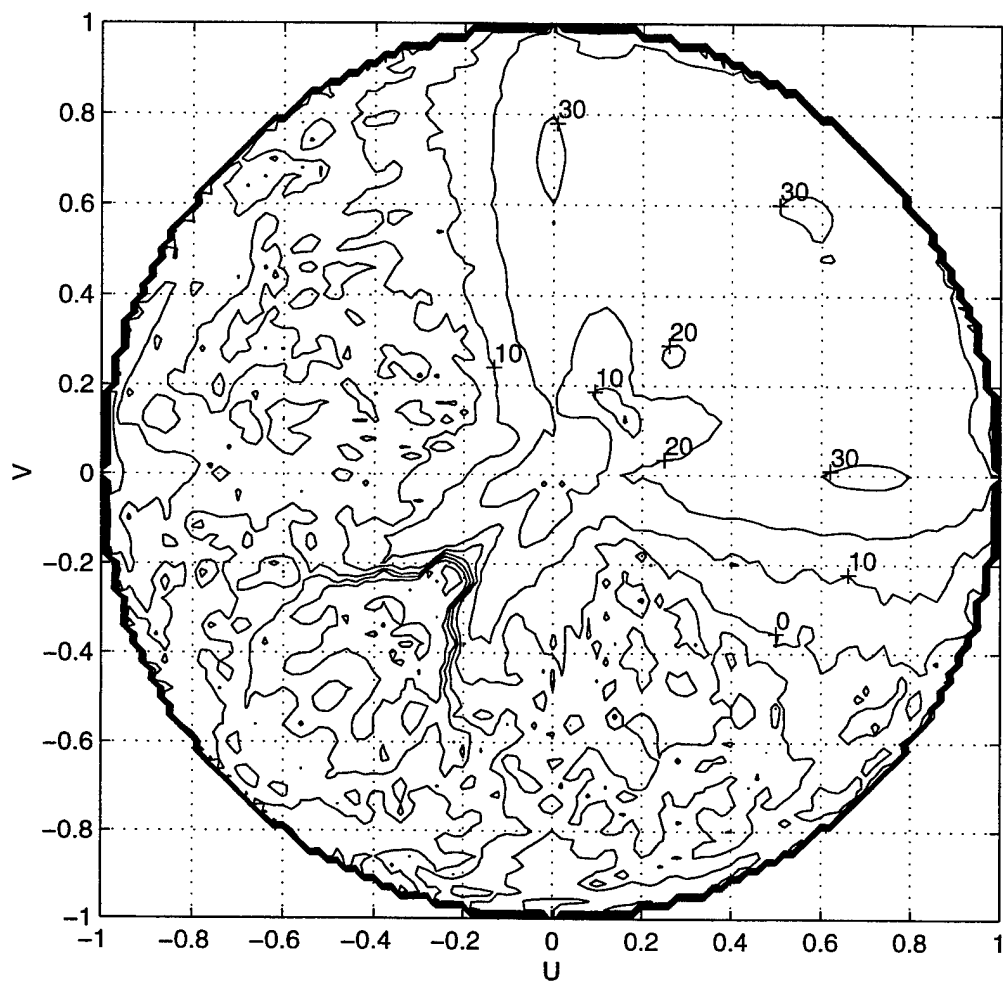
Figure 17. RCS of three triangular plate geometry at frequency of 60 MHz and 20 edges/side for $\theta = 60°$ using **Patch**.
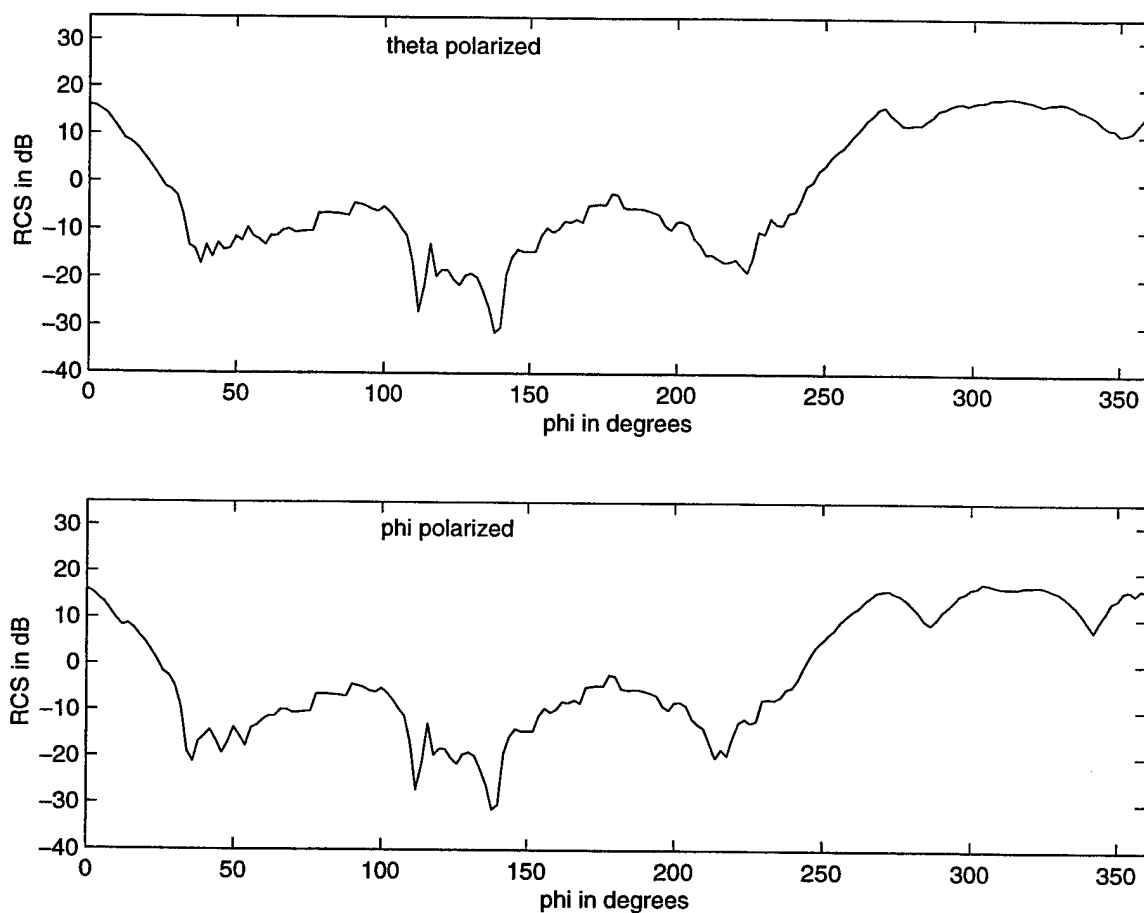
Figure 18. RCS of three triangular plate geometry at frequency of 60 MHz and 20 edges/side for $\theta = 60°$ using **Xpatch**.
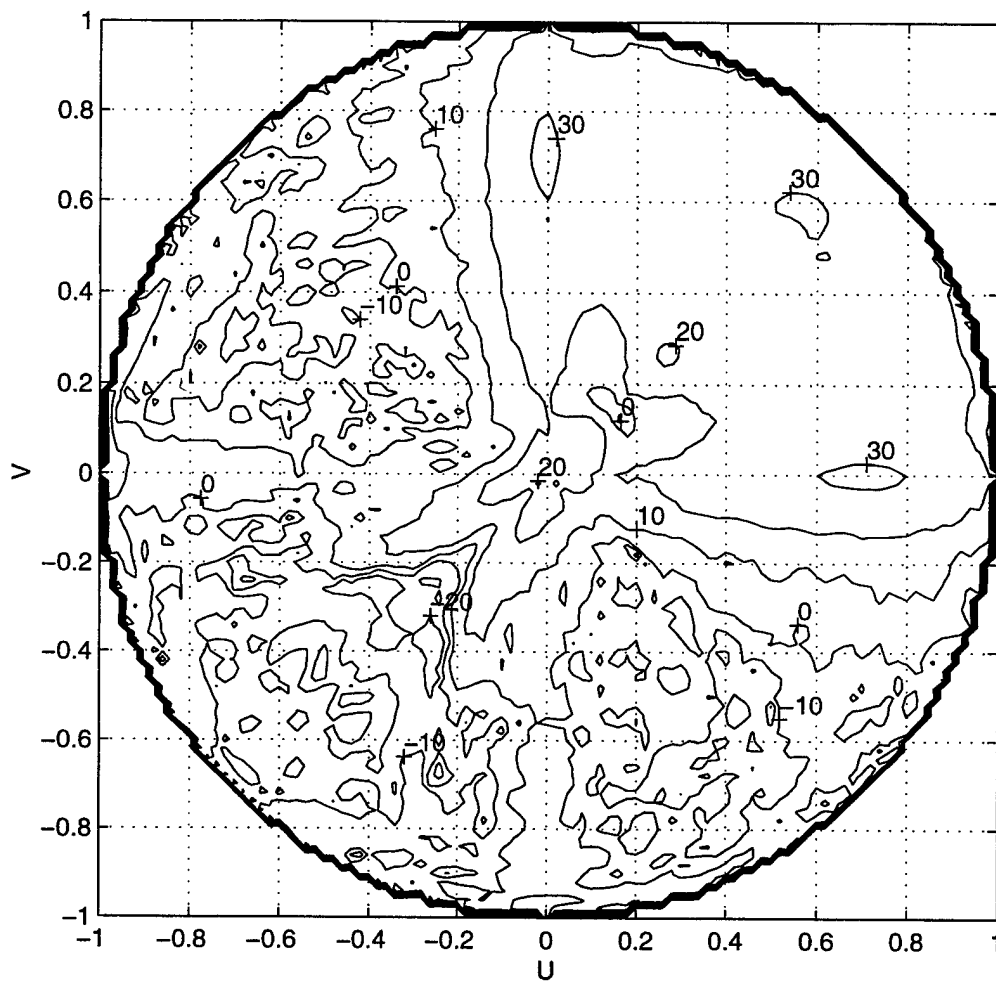
40

Figure 19. RCS of three triangular plate geometry at frequency of 120 MHz and 25 edges/side using **Xpatch**.

41

Figure 20. RCS of three triangular plate geometry at frequency of 120 MHz and 1 edge/side using **Xpatch**.

comparison of the plots it is seen that there are no differences, which implies that the segmentation is not an important factor in the calculation of RCS in **Xpatch** code. This is expected because the " soft" edges inside of the plate do not contribute to scattering. However, the calculation can take significantly longer (about 10 times) when small triangles are used because reflections must be computed between a larger number of patches. Finally, the edge diffraction does not affect the calculation of RCS as shown in Figure 21.

The effect of the number of facets in the **Patch** model was also checked. Two separate cases of plate segmentation were examined for a frequency of 120 MHz: (1) for 25 edges/side, and (2) for 20 edges/side. The result for (1) is shown in Figure 22. From the comparison of Figures 15 and 22 it is seen that there are only small differences, which implies that the segmentation is not an important factor at this frequency in the calculation of RCS in **Patch** code.

Figure 21. RCS of three triangular plate geometry at frequency of 120 MHz and 1 edge/side with edge diffraction using **Xpatch**.
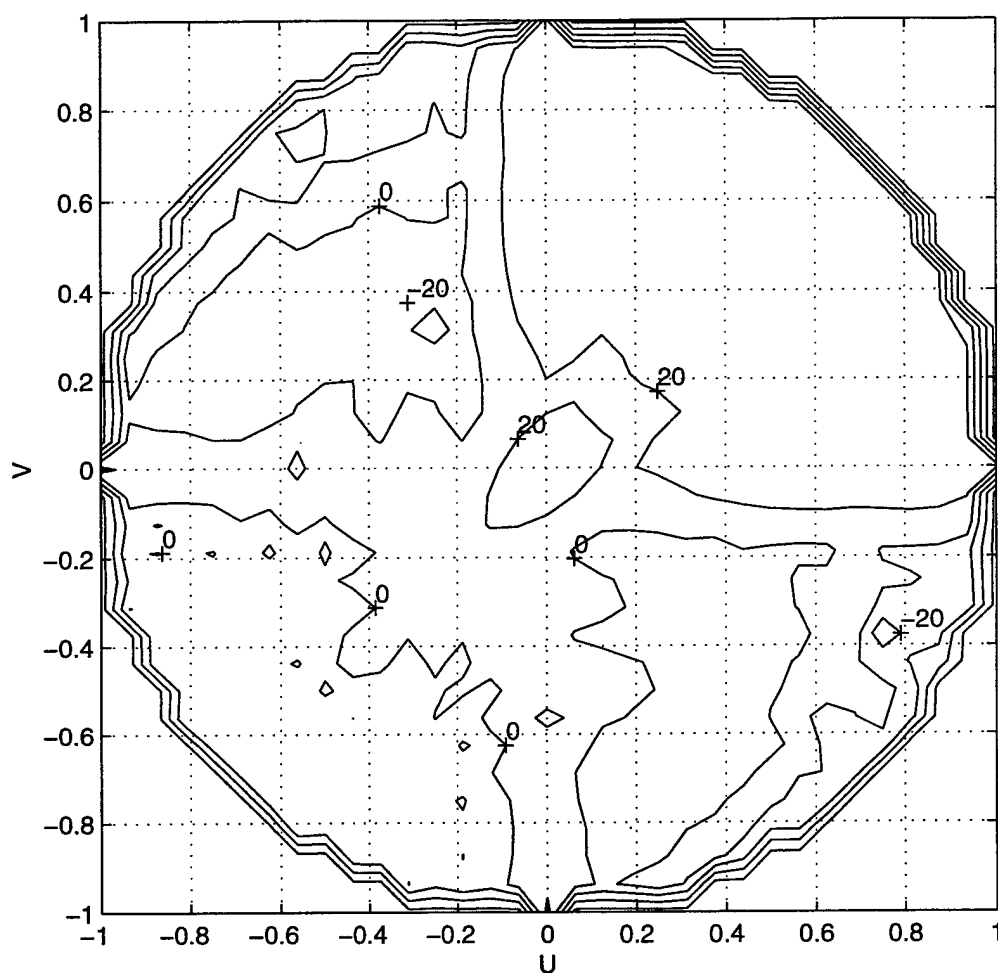
Figure 22. Three triangular plate geometry at frequency of 120 MHz and 25 edges/side using **Patch**.

D. COMPARISON OF RCS VALUES

The last step is to compare the highest RCS values that come from the codes with those from the formulas of Figure 4. The results for the rectangular and triangular cases are included in Table 2 and show that in general the values are in agreement, especially for higher frequencies. All of the RCS values are normalized by λ^2.

Table 2. Theoretical and computed maximum RCS in dB.

Plate Shape	60 MHz		120 MHz		240 MHz	
	codes	formulas	codes	formulas	codes	formulas
Rectangular	25.54	27.81	39.42	39.84	58.17	51.88
Triangular	18.55	18.26	31.53	30.30	43.87	42.34

V. CONCLUSIONS

In this thesis the RCS performance of three retroreflector geometries was examined. The RCS of the above geometries was computed for a range of frequencies using the CEM codes **Patch** and **Xpatch.** The results showed that in general the two codes agree in both the level of RCS as well as the spatial sectors where these values occur. The agreement increases with the frequency since the ray approach of **Xpatch** is based on high frequency techniques. One limitation for convergence of **Patch** is that the edge length should not exceed 0.1λ. However, it was found for the geometries under consideration here that a maximum edge length of 0.2λ could be tolerated. The segmentation is a factor that does not affect the RCS in **Xpatch** code.

As expected, the RCS increases with the effective area of the retroreflector. The highest RCS values from these two codes are in agreement with those from the theoretical expressions and this verifies the utility of the formulas. Although there are some differences between the two codes (given that they are based on different calculation and

47

methods), the use of either **Patch** or **Xpatch** is an accurate convenient way for predicting retroreflector RCS.

The triangular plate structure has lower RCS compared to the circular and rectangular plate structures. In many applications the triangular arrangement is preferred because of its smaller volume compared to the other two. Smaller volume has reduced weight, wind resistance, and is less unsightly than a large package. Thus the ratio

$$\frac{\text{High RCS Solid Angle}}{\text{Volume}}$$

could serve as a figure of merit for evaluating retroreflectors.

The question arises: how small can a retroreflector become yet still provide a sufficiently high RCS? From the calculated data it appears that 2λ edges are about the minimum for a good retroreflector. Below that the RCS pattern tends to be relatively isotropic. In the range of 2λ to 4λ edge lengths either of the simple three plate reflectors are efficient. When limited to this size range, other more complicated shapes do not significantly improve the RCS solid angle to volume ratio.

LIST OF REFERENCES

1. Jenn, D. C., *Radar and Laser Cross Section Engineering*, AIAA Series, AIAA, Washington, DC, 1995

2. Ruck, G. T., *Radar Cross Section Handbook*, vol. 2, Plenum Press, New York, NY, 1970

3. Hoisington, D. B., *ELECTRONIC WARFARE HANDBOOK*, Naval Postgraduate School, Monterey, CA, 1980

4. Ling, H., Chou, R. C., and Lee, S. W., "Shooting and Bouncing Rays: Calculating the RCS of an Arbitrarily Shaped Cavity", *IEEE Transactions on Antennas and Propagation*, vol.AP-37, No. 2, Feb. 1989

INITIAL DISTRIBUTION LIST

1. Defense Technical Information Center 2
   8725 John J. Kingman Rd., STE 0944
   Ft. Belvoir, Virginia 22060-6218

2. Dudley Knox Library...............................2
   Naval Postgraduate School
   411 Dyer Rd.
   Monterey, California 93943-5121

3. Chairman, Code EC...............................1
   Department of Electrical and Computer Engineering
   Naval Postgraduate School
   Monterey, California 93943-5121

4. Prof. David C. Jenn, Code EC/Jn.....................1
   Department of Electrical and Computer Engineering
   Naval Postgraduate School
   Monterey, California 93943-5121

5. Prof. Phillip E. Pace, Code EC/Pc...................1
   Department of Electrical and Computer Engineering
   Naval Postgraduate School
   Monterey, California 93943-5121

6. Embassy of Greece.................................1
   Naval Attache
   2228 Massachusetts Ave., NW
   Washington, DC 20008

7. Eleftherios I. Keroglou.............................2
   Hbis 3 St.
   16346 Hlioupoli
   Greece